

Atomistic Simulations of Defects Production under Ion Irradiation in Epitaxial Graphene on SiC

Mitisha Jain,* Silvan Kretschmer, Katja Höflich, Joao Marcelo Jordao Lopes, and Arkady V. Krasheninnikov*

Using first-principles and analytical potential atomistic simulations, production of defects in epitaxial graphene (EG) on SiC upon ion irradiation for ion types and energies accessible in helium-ion microscope is studied. Graphene-SiC systems consisting of the buffer (zero) graphene layer and SiC substrate, as well as one (monolayer) and two (bilayer) additional graphene layers, are focused on. The probabilities for single, double, and more complex vacancies to appear upon impacts of energetic ions in each graphene layer as functions of He- and Ne-ion energies are calculated and the data are compared with those obtained for free-standing graphene. The results indicate that the role of the substrate is minimal for He-ion irradiation with energies above 5 keV, which can be associated with a low sputtering yield from this system upon ion irradiation, as compared with the common Si/SiO₂ substrate. In contrast, SiC substrate has a significant effect on defect production upon Ne-ion irradiation. The results can serve as a guide to the experiments on ion irradiation of EG to choose the optimum ion beam parameters for defect-mediated engineering of such systems, for example, for creating nucleation centers to grow other 2D materials, such as h-BN, on top of the irradiated EG.

1. Introduction

The irradiation response of SiC materials, including both bulk SiC and epitaxial graphene (EG) on SiC, has received substantial amount of attention in the context of various applications. In particular, bulk SiC, existing as more than a hundred different polytypes, has been studied extensively in the past decades, as SiC composites are known for their excellent radiation tolerance,^[1,2] with potential applications as nuclear fission and fusion materials, as also atomistic simulations indicate.^[3,4] At high

temperatures, the metastable cubic polytype transforms to the hexagonal polytype,^[5] a conversion observed also at lower temperatures under neutron irradiation.^[6] Furthermore, applications of bulk SiC with irradiation-induced defects in the field of quantum computing have been demonstrated. Using ion irradiation, point defects in SiC polytypes can be created, which exhibit electronic spin states with long coherence time forming spin qubits.^[7,8]

The second subsystem of interest is EG on SiC,^[9] which possesses many advantages over graphene prepared by exfoliation^[10] and chemical vapor deposition^[11] techniques, including the fact that it does not require transfer to another substrate (e.g., for device applications), given the insulating nature of SiC. In addition, EG can also be patterned and modified by irradiation.^[12–14] In particular, swift heavy-ion irradiation has been used to optimize EG for the purpose of gas sensing.^[15]

Moreover, ion impacts were reported to change graphene behavior from n-doped to p-doped, so that ion bombardment can be used to tailor the properties of the system for electronic applications.^[16]

During the growth of EG on SiC, a buffer layer (here: zero-layer graphene, ZLG) is formed, which exhibits a hexagonal lattice as graphene but it is covalently bonded to the substrate. The structure and electronic properties of ZLG have been studied extensively both experimentally^[17–19] and theoretically.^[20–26] The bonded ZLG possesses the electronic structure which differs from that of

M. Jain, S. Kretschmer, A. V. Krasheninnikov
Institute of Ion Beam Physics and Materials Research
Helmholtz-Zentrum Dresden-Rossendorf
Bautzner Landstraße 400, 01328 Dresden, Germany
E-mail: m.jain@hzdr.de; a.krasheninnikov@hzdr.de

K. Höflich
Helmholtz-Zentrum Berlin für Materialien und Energie GmbH
14109 Berlin, Germany

K. Höflich
Ferdinand-Braun Institut gGmbH
Leibniz-Institut für Höchstfrequenztechnik
12489 Berlin, Germany

J. M. J. Lopes
Paul-Drude-Institut für Festkörperelektronik
Leibniz-Institut im Forschungsverbund Berlin e.V.
12489 Berlin, Germany

A. V. Krasheninnikov
Department of Applied Physics
Aalto University
P.O. Box 11100, FI-00076 Aalto, Finland

The ORCID identification number(s) for the author(s) of this article can be found under <https://doi.org/10.1002/pssr.202200292>.

© 2022 The Authors. physica status solidi (RRL) Rapid Research Letters published by Wiley-VCH GmbH. This is an open access article under the terms of the Creative Commons Attribution License, which permits use, distribution and reproduction in any medium, provided the original work is properly cited.

DOI: 10.1002/pssr.202200292

free-standing graphene. ZLG exhibits a large bandgap and the pinning of the Fermi level by a conduction band for the Si-terminated face.^[20,21] However, the missing Dirac cones emerge in the next graphene layer. We refer to this system as monolayer graphene (MLG).

The possibility of growing 2D materials on top of each other to form van der Waals heterostructures has been demonstrated.^[27,28] The thereby-realized heterostructures are promising for various devices architectures including atomically thin transistors. For this type of epitaxial growth, usually known as vdW epitaxy, nucleation can take place at surface features such as defects and surface steps.^[29] In a recent study, h-BN islands were grown on EG with spatial control, using a focused ion beam (FIB) within a helium-ion microscope (HIM) to precisely control defect production and engineer nucleation sites.^[30] At the same time, while EG on SiC obviously represents an interesting 2D material with numerous applications, its response to impacts of He ions in the HIM has not been fully understood. It can be different from that in free-standing graphene, as recently demonstrated for various supported 2D materials on SiO₂^[31] or metal^[32] substrates.

In this work, using atomistic simulations at the analytical potential and density functional theory (DFT) levels, we theoretically study defect production in EG on SiC under impacts of He and Ne ions. We explicitly account for the effects of the substrate (bulk SiC) on the response of graphene to irradiation. Since the substrate affects the number of displaced carbon atoms and vacancy types in EG, we present information about the number, types, and location of defects produced in each layer of EG to guide the experiment in tailoring the defect production.

2. Computational Details

Prior to carrying out massive analytical potential molecular dynamics (APMD) simulations, we tested the accuracy of the potential available for SiC in the context of defect energetics, because the choice of the potential is crucial for the assessment of the number of defects produced in the material under irradiation, as shown previously, for example, for MoS₂.^[33]

2.1. DFT Calculations

All the structures were studied within the framework of DFT as implemented in Vienna Ab initio Simulation Package.^[34–37] The semilocal exchange–correlation functional of Perdew–Burke–Ernzerhof^[38] (PBE) was used. The DFT-D3 method^[39] was selected to describe the long-range van der Waals interactions. The kinetic energy cutoff was set to 400 eV. At first, the properties of the bulk SiC system were studied. The calculated lattice parameters for bulk 4H-SiC (0001) ($a = 3.08805 \text{ \AA}$ and $c = 10.109 \text{ \AA}$) were found to be close to the values given in the literature.^[26] Similarly, the calculated lattice parameter for graphene is 2.46 \AA . Due to computational limitations, we adopted a 4×4 SiC model instead of the real $6\sqrt{3} \times 6\sqrt{3}R30^\circ$ (6R3) reconstruction model, as done previously, see the study by Markevich et al.^[26] for the comparison of the models. The coincidence lattice mismatch in this approximate model is 0.42%. A supercell of 5×5 graphene adsorbed on 4×4 SiC was constructed. The substrate consisted of four Si–C layers, as shown in **Figure 1a**. The dangling bonds at the bottom C

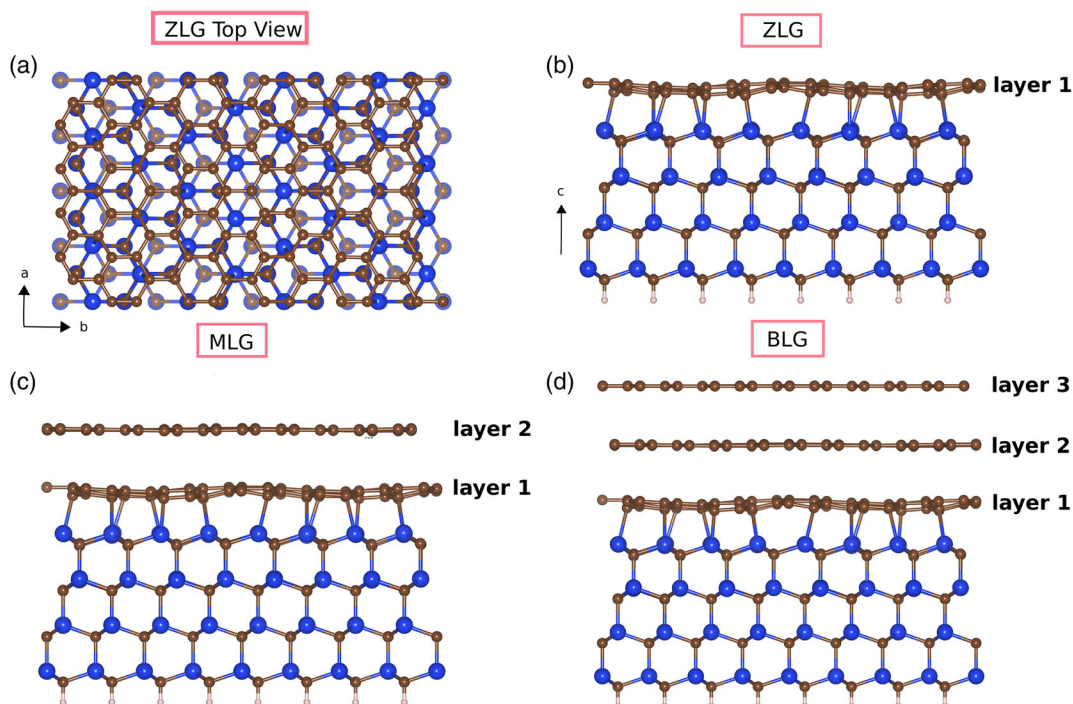


Figure 1. a) The top view of the optimized 5×5 graphene 4×4 Si–C model adopted in this work. Only the first SiC bilayer and ZLG are shown for clarity. b–d) The optimized supercells of ZLG, MLG, and BLG systems on top of SiC consisting of one, two, and three layers of graphene, respectively. The Si, C, and H atoms are represented as blue, brown, and pink balls, respectively.

atoms were saturated with hydrogen atoms. A vacuum of about 14 Å was added between the periodic images of the system in the z-direction. Three sets of calculations were performed. In each of them, an additional layer of graphene was added on top of the surface. Thus, we obtain ZLG, MLG, and bilayer graphene (BLG) systems with one, two, and three graphene layers, respectively (see Figure 1b–d). The $4 \times 4 \times 1$ Γ -centered k-point mesh was used. All the structures were relaxed until the Hellman–Feynmann forces were below 10^{-3} eV Å⁻¹, and the energy difference in the electronic self-consistent field was below 10^{-6} eV.

2.2. Analytical Potential Molecular Dynamics Simulations

The APMD simulations were performed using the LAMMPS^[40] package. The Tersoff^{ff[41,42]} potential was used to describe the interactions between Si–Si, Si–C, C–C atoms, and Ziegler–Biersack–Littmark^[43] (ZBL) potential for the interaction of He/Ne ions with other atoms in the system. The standard 12/6 Lennard–Jones potential between the C atoms with $\epsilon = 0.0027$ eV and $\sigma = 3.393$ Å was used to account for the long-range interactions in the multilayer graphene systems. A large simulation cell of dimensions 128 Å × 126 Å × 100 Å was constructed for each system type. The thickness of the slab was chosen by performing transport of ions in matter (TRIM) simulations^[44] for a slab hundreds of nm thick and determining from which depth the energetic recoils can reach the surface. The SiC system consisted of eight Si–C bilayers placed below the graphene layers. Test calculations for the thicker substrate gave the same result within the statistical error. Periodic boundary conditions were applied in the x- and y-directions. Before performing any irradiation simulations, all the structures were carefully optimized using the conjugate gradient algorithm. The energy dissipation during ion impact simulations was performed using a Berendsen thermostat.^[45] Three thermostat regions were constructed around the boundary atoms as described previously.^[46] The irreducible area was chosen to simulate defects produced under impacts of energetic ions. 378 impact points were then used to simulate the outcome of single-ion impact statistically. Notably, these simulations reflect the irradiation of the material in the single-impact limit corresponding to low fluences (6.2×10^{11} ions cm⁻²), in which the probability that the ion hits the same spot is negligibly small. The time step varied depending on the maximum velocity of the atoms in the system. The

maximum distance travelled during one time step was set to 0.001 Å, and the time step was calculated accordingly, falling in the range from about 10^{-4} fs for He ions with maximum energies (in the beginning of the run) up to 0.1 fs. The impact simulation was followed by quenching of the system and analysis of the atomic structure. The total run time for any simulation was about 25 ps. We consider ion energies in the range of 5–30 keV, which can be used (although at the cost of a partial loss of spatial resolution at low energies) in HIM experiments. We neglected the effect of step edges on defect production, as their concentration should be relatively low, and our simulation cell was definitely smaller than the typical micrometer-sized SiC plateau observed in the experiments.

3. Results and Discussions

3.1. DFT Versus APMD Simulations

In this section, we will compare the results for structural parameters and binding energies calculated using the DFT and APMD approaches. Using DFT and Tersoff potential calculations, the binding energies of ZLG to the Si–C substrate are found to be -0.12 and -0.14 eV per carbon atom, respectively (see **Table 1**). Both values are slightly lower as compared to the local-density approximation (LDA)^[26] and local spin density approximation (LSDA)^[20] values. However, it is expected that the LDA overestimates the binding energy.^[47] The adsorption distances calculated using both DFT (2.28 Å) and Tersoff potential (2.29 Å) are quite similar. However, the corrugation heights (maximum displacement of graphene carbon atoms in z-direction) of ZLG differ significantly from both techniques (0.65 and 1.27 Å). From DFT, the top layers are extremely flat in MLG and BLG systems with corrugation heights of 0.13 and 0.02 Å, respectively. However, Tersoff + LJ overestimates these values (0.39, 0.09 Å). In addition, the binding energies for these layers (0.11, 0.17 eV) are estimated to be higher than the DFT-calculated values (0.06 eV). From experimental studies, the corrugations in ZLG and MLG are determined as around 0.52–1 and 0.29–0.4 Å, respectively.^[48,49] The C–C interplanar distances are in the range of 3.38–3.42 Å (DFT) and 3.20–3.27 Å (Tersoff + LJ).

Next, we assessed the formation energies of single vacancies E_f in ZLG by removing carbon atoms at different locations; see **Figure 2a**. E_f was calculated using the following equation

Table 1. Structural properties calculated using DFT and analytical potentials for top layers of ZLG, MLG, and BLG systems, along with the results available in the literature. Here, h is the average adsorption distance/c–c interplanar distance, Δh is the maximum corrugation height and E_b is the binding energy of graphene per C atom.

Method	ZLG			MLG			BLG		
	h [Å]	Δh [Å]	E_b [eV]	h [Å]	Δh [Å]	E_b [eV]	h [Å]	Δh [Å]	E_b [eV]
PBE+vdW	2.28	0.65	0.12	3.42	0.13	0.06	3.38	0.02	0.06
MD	2.29	1.27	0.14	3.27	0.39	0.11	3.26	0.09	0.17
LDA ^[26]	2.22	0.52	0.18	–	–	–	–	–	–
LSDA ^[20]	2.58	–	0.17	3.30	–	–	–	–	–
PBE+vdW ^[25]	2.32	0.83	–	3.40	0.41	–	3.37	0.24	–
Perdew–Wang ^[22]	–	1.20	–	–	0.40	–	–	–	–

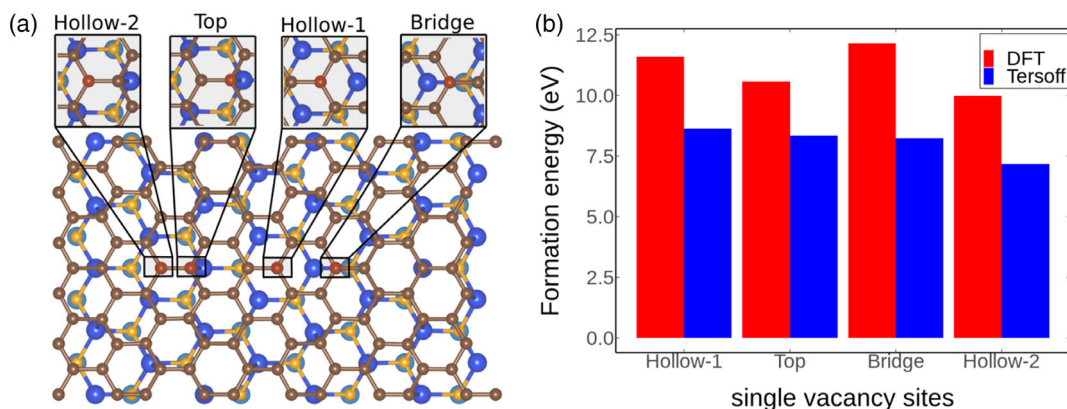


Figure 2. a) The pictorial representation of different vacancy sites. Only top two SiC layers are shown for clarity. The ZLG C atoms are shown in brown. The atoms shaded in red were removed to create C vacancies. The C atoms in SiC are shown in yellow. The blue and light blue atoms are Si of first and second layer, respectively. b) The defect formation energies calculated for ZLG with respect to different single-vacancy sites using PBE–DFT and Tersoff potential.

$$E_f = E_{N-1} - E_N + \mu(C) \quad (1)$$

where E_{N-1} and E_N are the energies of the defective and pristine system after geometry optimization, respectively. As we are interested in the formation of defects under ion irradiation, but not at their equilibrium concentration at finite temperatures, the chemical potential of carbon atom $\mu(C)$ was chosen to correspond to the energy of an isolated atom. In the above equation, $\mu(C)$

equals -1.32 eV as DFT calculations yield, and it is zero in the analytical potential approach.

E_f values for single vacancies are in the range of 10.0–12.1 eV (DFT) and 7.2–8.6 eV (Tersoff). The single-vacancy formation energies for ZLG are lower than those for free-standing graphene (≈ 15.24 eV). This can be expected, as bonding of graphene to a substrate lowers the formation energy.^[32] The lowest DFT-calculated formation energy is for the Hollow-2 site (≈ 10.0 eV), where sp^2 carbon atom is bonded to three other

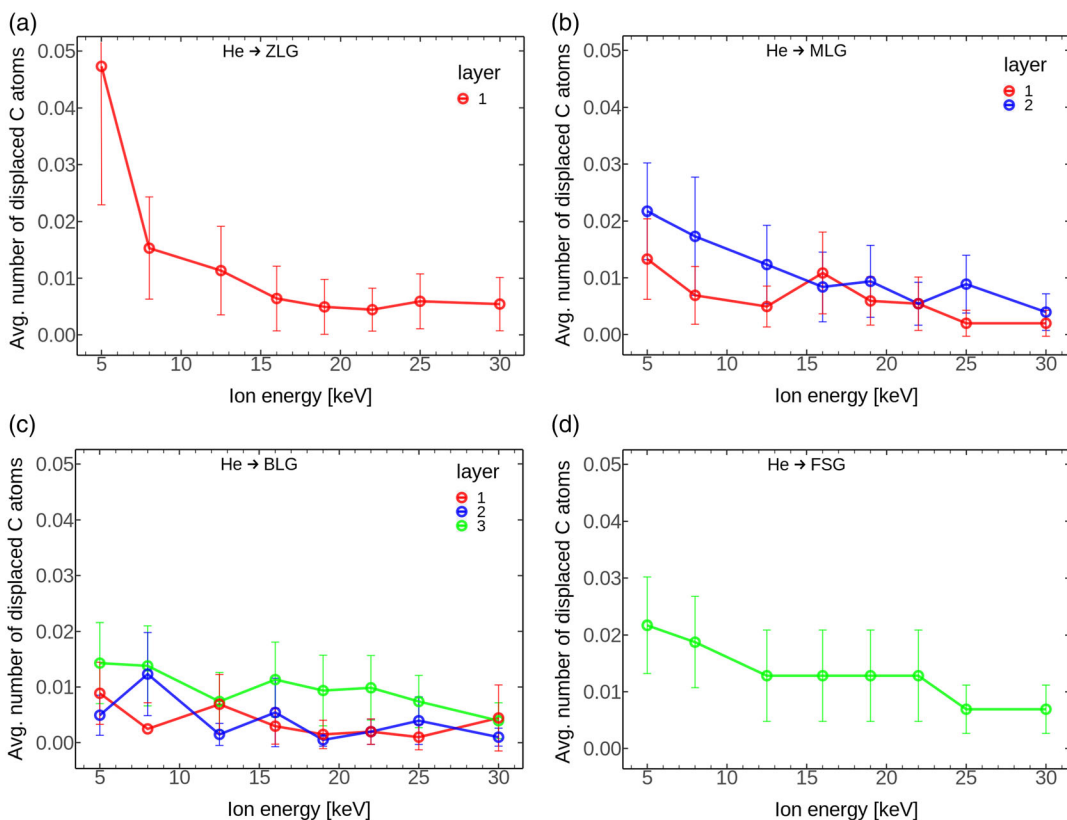


Figure 3. The average number of displaced carbon atoms from a–c) different graphene layers of the ZLG, MLG, BLG systems and d) free-standing single-layer graphene as a function of He-ion energies. The error bars are the standard deviations from the mean value.

sp^3 carbon atoms. The next lowest formation energy site is found for the sp^3 carbon atom (bonded) on top of the silicon atom (≈ 10.6 eV). The resultant reconstruction is similar to what has been previously reported.^[50] Both Hollow-1 (≈ 11.6 eV) and Bridge (≈ 12.1 eV) sites have a higher formation energy as the sp^2 carbon atom is bonded to three other sp^2 carbon atoms. From Figure 1b, it is apparent that the Tersoff potential gives the values of E_f which are in qualitative agreement with the DFT values, but it underestimates vacancy formation energies in ZLG, so that the concentration of irradiation-induced defects assessed using this potential may be higher than what one can envisage using the DFT results. Moreover, the ion energies simulated in this work are rather high, giving rise to the energies transferred to the recoil atoms that are on average substantially higher than the E_f values, so that one can conclude that the Tersoff potential is overall suitable for carrying out the irradiation simulations of the graphene–SiC system.

3.2. Average Number of Carbon Atoms Displaced upon He-/Ne-Ion Impacts

Having compared the structural properties and single-vacancy formation energies obtained using the DFT and Tersoff potential simulations, we proceed with the discussion of the results of ion irradiation simulations. Here, we present the layer-wise analysis of the defects produced in the ZLG, MLG, and BLG systems. For

that, we considered beam energies of 5, 8, 12.5, 16, 19, 22, 25, and 30 keV. In Figure 3 and 4, the average number N_n of carbon atoms displaced from a graphene layer with index n per He-/Ne-ion impact is presented. Atoms were considered to be displaced from the layer if the separation between the initial and final positions (in z -axis) was more than 2.1 \AA .

For He, the number of atoms displaced from the top layers in ZLG, MLG, and BLG systems decreases with increasing ion energies. Such a behavior is typical for 2D materials including graphene,^[51] h-BN^[52,53], MoS₂^[31,33], and black phosphorus^[54] sheets. The reason for the drop in the number of defects has been discussed previously at length, see Ref. [55] and references therein. It is related to a decrease in the cross section for atom displacement at higher energies of the projectiles. In contrast, all ion energy is eventually transferred to defects and heat in the bulk system, but more defects are produced with increasing energy, although deeper in the sample. Correspondingly, at higher energies, more defects will be produced in SiC, but not in graphene. In case of ZLG, $N_1^{\text{ZLG}} \approx 0.05$ is found at lower energies such as 5 keV. At the same time, in the energy range of 8–30 keV, N_1^{ZLG} lies between 0.004 and 0.015. In contrast to ZLG, for MLG and BLG, only slight decrease in N_2^{MLG} and N_3^{BLG} is observed at energies above 5 keV. Hence, one can conclude that the substrate weakly affects the defect production in graphene for He-ion energies higher than 5 keV. This can be associated with a smaller sputtering yield from SiC, as compared to, for example,

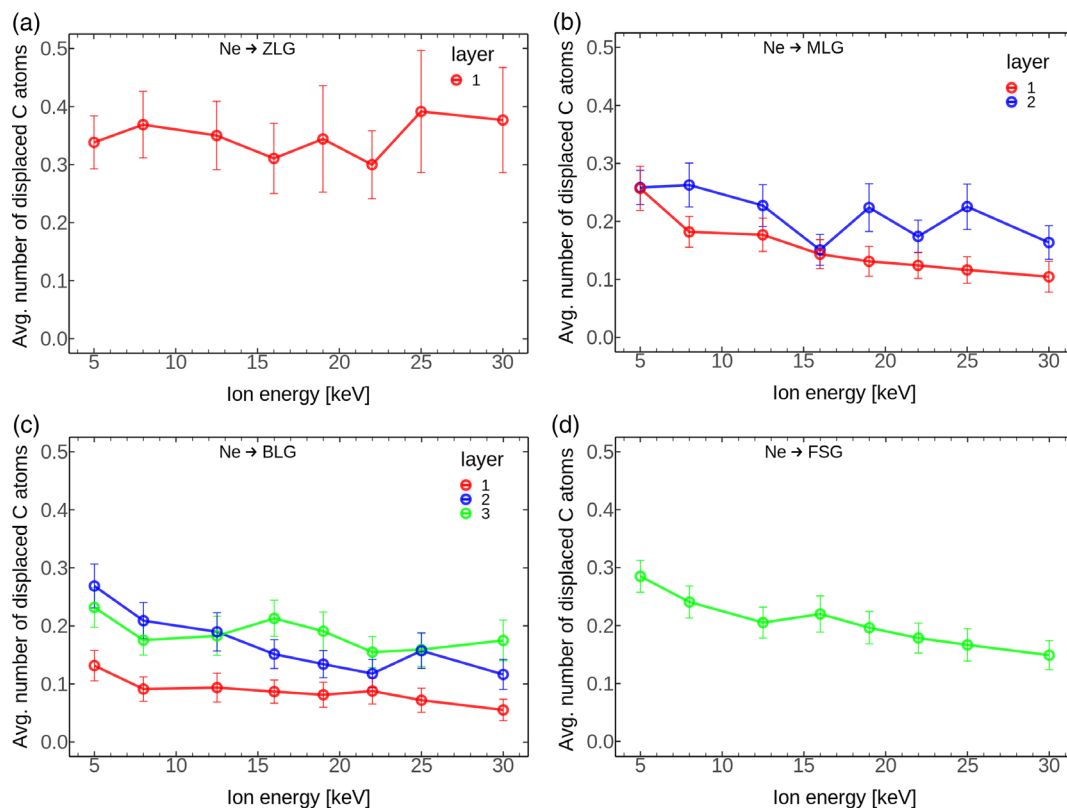


Figure 4. The average number of displaced carbon atoms from a–c) different graphene layers of the ZLG, MLG, BLG systems and d) FSG as a function of Ne-ion energies. The error bars are the standard deviations from the mean value.

SiO₂. Indeed, our simulations using the code TRIM^[44] gave the following values for the total sputtering yield from SiO₂ and SiC substrates under 30 keV He-ion irradiation: $Y_{\text{SiC}} = 0.18$ and $Y_{\text{SiO}_2} = 0.47$. We note that for ZLG about 60% of the displaced atoms are sputtered away, that is, left the sample, which also emphasizes the important role of the SiC substrate.

We note that the presence of the substrate reduces the number of defects produced directly by impacts of energetic ions, as evident from the comparison of the BLG and free-standing

graphene, but at high energies of He ions, most defects are produced by atoms sputtered from the substrate, as shown previously.^[31] We also note that the sputtering yield depends on ion energy. At energies above 10 keV the defect numbers are comparable to the values obtained previously in the simulations of the irradiation of free-standing graphene.^[51] The effect of the substrate is apparently manifested in the absence of Stone–Wales defects reported for free-standing graphene.^[56]

On the other hand, in case of heavier Ne ions, the substrate effects in displacing C atoms are clearly noticeable. The N_1^{ZLG} values are much higher than N_2^{MLG} (0.26–0.15) and N_3^{BLG} (0.23–0.15) for the energy range considered in this study. The N_1^{ZLG} (0.39–0.30) values are constant in the range of 5–30 keV, which is clearly different for the free-standing graphene, where the values decrease with ion energy.^[51] The observed trend is as follows: $\text{BLG}(3) \approx \text{MLG}(2) < \text{ZLG}(1)$. In this case, the increase in number of graphene layers in the system reduces the substrate effect.

3.2.1. Finite-Temperature Irradiation Simulation

So far we have not studied the role temperature plays in defect production. In addition to the simulations performed at $T = 0$ K, we also carried out simulations at room temperature $T = 300$ K and compared the results obtained for the case where MLG system was irradiated with Ne ions. Prior to irradiation, the system was thermalized at 300 K. The thermostat regions were also kept

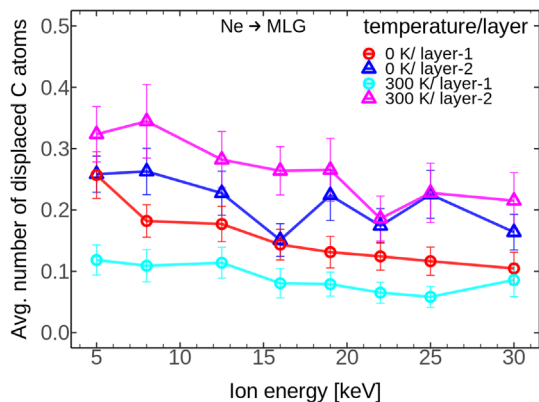


Figure 5. Average number of displaced carbon atoms from MLG system at zero and room (300 K) temperature as functions of Ne-ion energy.

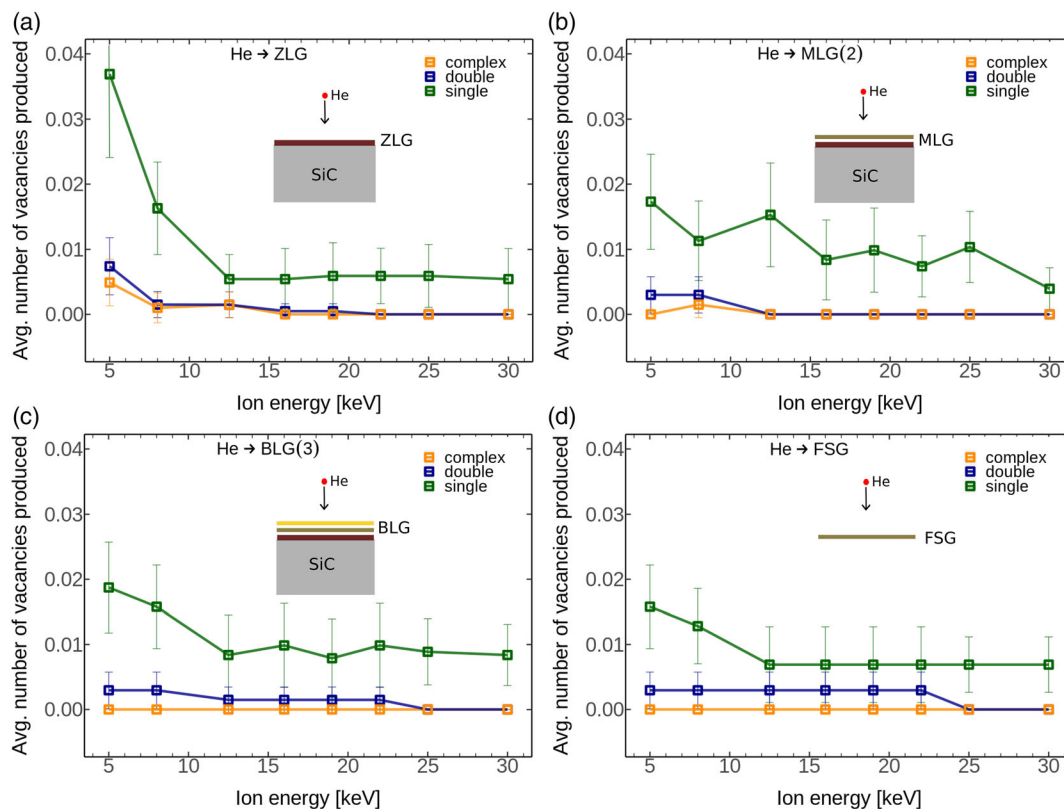


Figure 6. a–d) The average number of different types of vacancies (single, double, and complex) produced from single He-ion impact in the top graphene layer present in ZLG, MLG, and BLG systems compared to free-standing graphene.

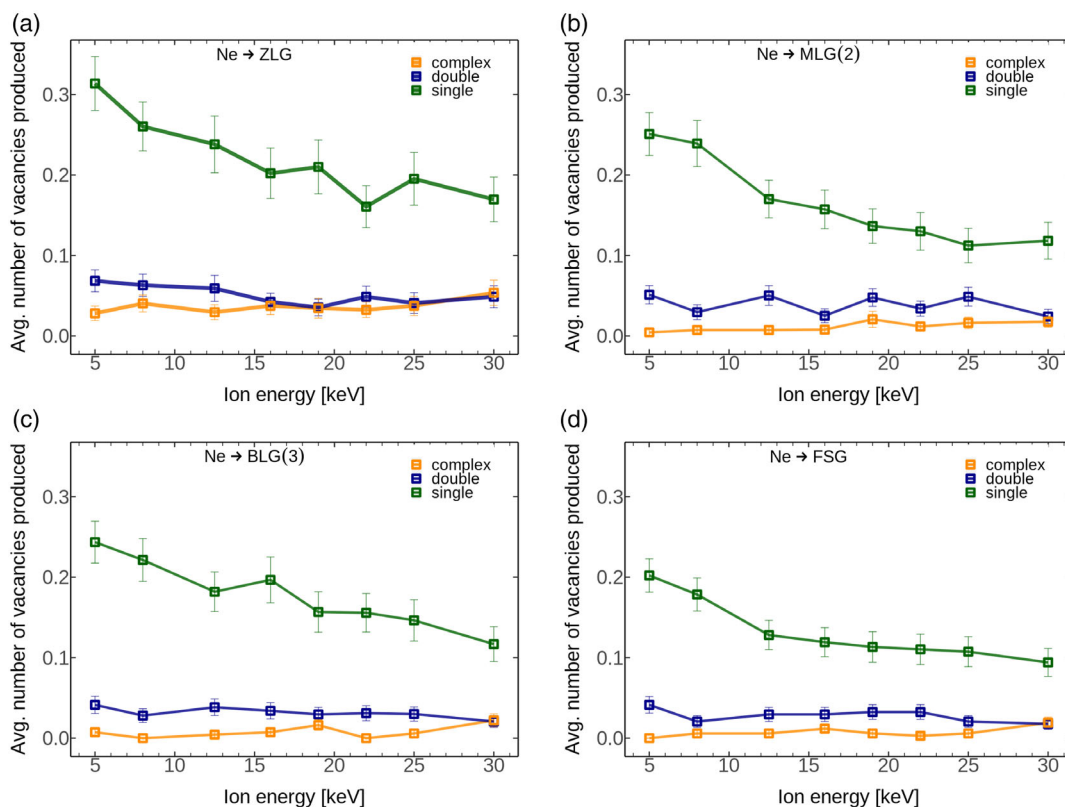


Figure 7. a–d) The average number of different types of vacancies (single, double, and complex) produced from single Ne-ion impact in the top graphene layer present in ZLG, MLG, and BLG systems compared to free-standing graphene.

at this temperature during the irradiation stage. The results are presented in **Figure 5**. It is evident that the number of defects in the buffer layer decreases due to in situ annealing of defects, but in the top layer increases, which can be associated with a higher backscattering rate of Ne atoms due to atom motion in SiC and also higher sputtering rate of the substrate atoms. For most energies, the absolute numbers differ by 30–50% with the difference being smaller for the experiment-relevant energies of 20–30 keV, while the trends in the sputtered atoms versus ion energy remain the same. Overall, as we aim at order-of-magnitude estimate of the concentration of irradiation-induced defects, one can state that the results are qualitatively the same.

3.3. Vacancy-Type Analysis and Comparison to Free-Standing Graphene

In **Figure 6** and **7**, the numbers of different types of vacancies (single, double, complex) produced by He- and Ne-ion impacts in the top layer of each system are compared. When the ZLG system is irradiated with He ions, mostly single vacancies are produced. At energies ≤ 19 keV, few occurrences of complex and double vacancies are seen. Similar results are obtained for other systems. The following trend is observed with respect to number of vacancies produced for each vacancy type: $N_{\text{complex}} < N_{\text{double}} < N_{\text{single}}$. As the substrate effects are minimal in case of He irradiation of BLG, the response of the BLG system

resembles that of the free-standing graphene. The number of single vacancies in free-standing graphene and BLG lies in the range of 0.007–0.016 and 0.008–0.019, respectively. The numbers of double vacancies are below 0.003 in both cases. Moreover, no complex vacancies are produced.

As evident from **Figure 7**, single vacancies are dominant also for Ne irradiation in the considered energy range. In case of ZLG system, the amounts of complex (0.03–0.05) and double (0.04–0.07) vacancies are larger than in the free standing graphene case (0.003–0.02 and 0.02–0.04, respectively), whereas BLG and MLG behave similarly to the free-standing graphene. The numbers of single, double, and complex vacancies in BLG are 0.12–0.24, 0.02–0.04, and 0–0.02, respectively. These values are close to those obtained for the free-standing graphene (single (0.1–0.2), double (0.02–0.04), and complex (0–0.02)). Similarly, this is also true for single (0.12–0.25), double (0.02–0.05), and complex (0.004–0.02) vacancies in MLG.

4. Conclusion

In conclusion, using atomistic simulations, we studied the effects of ion irradiation on graphene epitaxially grown on SiC. Keeping in mind the potentials of HIM for creating defects with subnanometer spatial resolution, we focused on ion energies and ion types accessible in HIM. We benchmarked the Tersoff potential against DFT calculations in the context of defect

energetics, and our results indicate that although the Tersoff potential gives a qualitatively correct picture, it underestimates defect formation energies, which means that the concentration of defects in the samples after irradiation can slightly be higher, as obtained in the APMD simulations. On the other hand, the in situ annealing of defects on the macroscopic timescale is not accounted for in our simulations, which may have the opposite effect. From previous studies it is known that the structural evolution of defects in sp²-bonded carbon materials includes migration of single vacancies^[57,58] and their coalescence into larger defects followed by Stone–Wales-like bond rotations.^[59,60] In multilayer graphene, annihilation of interstitials with vacancies is naturally expected. We note, though, that according to the DFT calculations, the efficient annealing of defects in graphitic systems requires elevated temperatures, around 300 °C, when single vacancies and bound interstitials become mobile,^[57,58,61–63] as also corroborated by experimental observations.^[64] Thus we expect that our calculations give qualitatively correct estimates of the number of defects in the system produced at room temperature. We further assessed the number of single, double, and more complex vacancies per ion impact of He and Ne ions produced in the graphene–SiC systems consisting of the buffer graphene layer and SiC substrate, as well as one and two additional graphene layers, and compared the data to those obtained for the free-standing graphene. We found that the role of the Si–C substrate is minimal for He-ion irradiation with energies above 5 keV. In contrast, SiC substrate has a significant effect on defect production upon Ne-ion irradiation. Our results can be used to guide the experiments on ion irradiation of EG and optimize the ion beam parameters (fluence, ion energy) for defect-mediated engineering of such systems, for example, for creating nucleation centers for growing new 2D materials such as h-BN on top of the irradiated EG.

Acknowledgements

The authors thank the HZDR Computing Center, HLRS, Stuttgart, Germany, and TU Dresden Cluster “Taurus” for generous grants of CPU time. The authors acknowledge the Leibniz Foundation (project ENGRAVE Nr. K335/2020) for support. A.V.K. also thanks the German Research Foundation (DFG) for funding through project KR 4866/6-1 and the collaborative research center “Chemistry of Synthetic 2D Materials” SFB-1415-417590517. The authors thank Dr. M. Ghorbani-Asl for fruitful discussions. The authors also thank the European Cooperation in Science and Technology (COST) action CA19140 “FIT4NANO” (<https://www.fit4nano.eu>) for support.

Open Access funding enabled and organized by Projekt DEAL.

Conflict of Interest

The authors declare no conflict of interest.

Data Availability Statement

The data that support the findings of this study are available from the corresponding author upon reasonable request.

Keywords

defects, epitaxial graphene, helium-ion microscopes, ion beam irradiation

Received: August 9, 2022

Revised: October 12, 2022

Published online: October 28, 2022

- [1] L. Snead, T. Nozawa, M. Ferraris, Y. Katoh, R. Shinavski, M. Sawan, *J. Nucl. Mater.* **2011**, *417*, 330.
- [2] S. Zinkle, L. Snead, *Annu. Rev. Mater. Res.* **2014**, *44*, 241.
- [3] D. Chen, F. Gao, B. Liu, *Sci. Rep.* **2015**, *5*, 16602.
- [4] M. Jiang, S. M. Peng, H. B. Zhang, C. H. Xu, H. Y. Xiao, F. A. Zhao, Z. J. Liu, X. T. Zu, *Sci. Rep.* **2016**, *6*, 20669.
- [5] S. Limpijumnong, W. R. L. Lambrecht, *Phys. Rev. B* **1998**, *57*, 12017.
- [6] C. M. Parish, T. Koyanagi, S. Kondo, Y. Katoh, *Sci. Rep.* **2017**, *7*, 1198.
- [7] A. L. Falk, B. B. Buckley, G. Calusine, W. F. Koehl, V. V. Dobrovitski, A. Politi, C. A. Zorman, P. X. L. Feng, D. D. Awschalom, *Nat. Commun.* **2013**, *4*, 1819.
- [8] Z. Shang, A. Hashemi, Y. Berencén, H.-P. Komsa, P. Erhart, S. Zhou, M. Helm, A. V. Krashennikov, G. V. Astakhov, *Phys. Rev. B* **2020**, *101*, 144109.
- [9] C. Berger, Z. Song, T. Li, X. Li, A. Y. Ogbazghi, R. Feng, Z. Dai, A. N. Marchenkov, E. H. Conrad, P. N. First, W. A. de Heer, *J. Phys. Chem. B* **2004**, *108*, 19912.
- [10] M. Yi, Z. Shen, *J. Mater. Chem. A* **2015**, *3*, 11700.
- [11] S.-M. Lee, J.-H. Kim, J.-H. Ahn, *Mater. Today* **2015**, *18*, 336.
- [12] H. Okumura, *Jpn. J. Appl. Phys.* **2006**, *45*, 7565.
- [13] F. Roccaforte, P. Fiorenza, G. Greco, R. L. Nigro, F. Giannazzo, A. Patti, M. Saggio, *Phys. Status Solidi A* **2014**, *211*, 2063.
- [14] F. Roccaforte, P. Fiorenza, M. Vivona, G. Greco, F. Giannazzo, *Materials* **2021**, *14*, 3923.
- [15] P. D. Kaushik, I. G. Ivanov, P.-C. Lin, G. Kaur, J. Eriksson, G. Lakshmi, D. Avasthi, V. Gupta, A. Aziz, A. M. Siddiqui, M. Syväjärvi, G. R. Yazdi, *Appl. Surf. Sci.* **2017**, *403*, 707.
- [16] O. Ochedowski, B. Kleine Bussmann, B. Ban d’Etat, H. Lebius, M. Schleberger, *Appl. Phys. Lett.* **2013**, *102*, 153103.
- [17] G. M. Rutter, J. N. Crain, N. P. Guisinger, T. Li, P. N. First, J. A. Stroscio, *Science* **2007**, *317*, 219.
- [18] C. Riedl, C. Coletti, U. Starke, *J. Phys. D: Appl. Phys.* **2010**, *43*, 374009.
- [19] T. W. Hu, F. Ma, D. Y. Ma, D. Yang, X. T. Liu, K. W. Xu, P. K. Chu, *Appl. Phys. Lett.* **2013**, *102*, 171910.
- [20] A. Mattausch, O. Pankratov, *Phys. Rev. Lett.* **2007**, *99*, 076802.
- [21] F. Varchon, R. Feng, J. Hass, X. Li, B. N. Nguyen, C. Naud, P. Mallet, J.-Y. Veuillen, C. Berger, E. H. Conrad, L. Magaud, *Phys. Rev. Lett.* **2007**, *99*, 126805.
- [22] F. Varchon, P. Mallet, J.-Y. Veuillen, L. Magaud, *Phys. Rev. B* **2008**, *77*, 235412.
- [23] L. Bellucci, T. Cavallucci, V. Tozzini, *Front. Mater.* **2019**, *6*, 198.
- [24] T. Cavallucci, V. Tozzini, *Sci. Rep.* **2018**, *8*, 13097.
- [25] L. Nemeč, V. Blum, P. Rinke, M. Scheffler, *Phys. Rev. Lett.* **2013**, *111*, 065502.
- [26] A. Markevich, R. Jones, S. Öberg, M. J. Rayson, J. P. Goss, P. R. Briddon, *Phys. Rev. B* **2012**, *86*, 045453.
- [27] M. Heilmann, M. Bashouti, H. Riechert, J. M. J. Lopes, *2D Mater.* **2018**, *5*, 025004.
- [28] M. Heilmann, A. S. Prikhodko, M. Hanke, A. Sabelfeld, N. I. Borgardt, J. M. J. Lopes, *ACS Appl. Mater. Interfaces* **2020**, *12*, 8897.
- [29] A. Azizi, S. Eichfeld, G. Geschwind, K. Zhang, B. Jiang, D. Mukherjee, L. Hossain, A. F. Piasecki, B. Kabius, J. A. Robinson, N. Alem, *ACS Nano* **2015**, *9*, 4882.

- [30] F. I. Allen, *Beilstein J. Nanotechnol.* **2021**, *12*, 633.
- [31] S. Kretschmer, M. Maslov, S. Ghaderzadeh, M. Ghorbani-Asl, G. Hlawacek, A. V. Krasheninnikov, *ACS Appl. Mater. Interfaces* **2018**, *10*, 30827.
- [32] S. Standop, O. Lehtinen, C. Herbig, G. Lewes-Malandrakis, F. Craes, J. Kotakoski, T. Michely, A. V. Krasheninnikov, C. Busse, *Nano Lett.* **2013**, *13*, 1948.
- [33] M. Ghorbani-Asl, S. Kretschmer, D. E. Spearot, A. V. Krasheninnikov, *2D Mater.* **2017**, *4*, 025078.
- [34] G. Kresse, J. Hafner, *Phys. Rev. B* **1993**, *47*, 558.
- [35] G. Kresse, J. Furthmüller, *Comput. Mater. Sci.* **1996**, *6*, 15.
- [36] G. Kresse, J. Furthmüller, *Phys. Rev. B* **1996**, *54*, 11169.
- [37] G. Kresse, D. Joubert, *Phys. Rev. B* **1999**, *59*, 1758.
- [38] J. P. Perdew, K. Burke, M. Ernzerhof, *Phys. Rev. Lett.* **1997**, *78*, 1396.
- [39] S. Grimme, J. Antony, S. Ehrlich, H. Krieg, *J. Chem. Phys.* **2010**, *132*, 154104.
- [40] A. P. Thompson, H. M. Aktulga, R. Berger, D. S. Bolintineanu, W. M. Brown, P. S. Crozier, P. J. in 't Veld, A. Kohlmeyer, S. G. Moore, T. D. Nguyen, R. Shan, M. J. Stevens, J. Tranchida, C. Trott, S. J. Plimpton, *Comp. Phys. Commun.* **2022**, *271*, 108171.
- [41] J. Tersoff, *Phys. Rev. B* **1989**, *39*, 5566.
- [42] G. Rajasekaran, R. Kumar, A. Parashar, *Mater. Res. Express* **2016**, *3*, 035011.
- [43] J. F. Ziegler, U. Littmark, J. P. Biersack, *The Stopping and Range of Ions in Solids* (J. F. Ziegler, J. P. Biersack, U. Littmark), Pergamon, New York **1985**.
- [44] J. F. Ziegler, J. P. Biersack, Program TRIM, **2008**, <http://www.srim.org> (accessed: October 2022).
- [45] H. J. C. Berendsen, J. P. M. Postma, W. F. van Gunsteren, A. DiNola, J. R. Haak, *J. Chem. Phys.* **1984**, *81*, 3684.
- [46] S. Ghaderzadeh, V. Ladygin, M. Ghorbani-Asl, G. Hlawacek, M. Schleberger, A. V. Krasheninnikov, *ACS Appl. Mater. Interfaces* **2020**, *12*, 37454.
- [47] Y. Wang, Z. Xu, Y. N. Moe, *Chem. Phys.* **2012**, *406*, 78.
- [48] S. Goler, C. Coletti, V. Piazza, P. Pingue, F. Colangelo, V. Pellegrini, K. V. Emtsev, S. Forti, U. Starke, F. Beltram, S. Heun, *Carbon* **2013**, *51*, 249.
- [49] T. Schumann, M. Dubsclaff, M. H. Oliveira, M. Hanke, J. M. J. Lopes, H. Riechert, *Phys. Rev. B* **2014**, *90*, 041403.
- [50] C. P. Huelmo, M. G. Menezes, R. B. Capaz, P. A. Denis, *Phys. Chem. Chem. Phys.* **2020**, *22*, 16096.
- [51] O. Lehtinen, J. Kotakoski, A. V. Krasheninnikov, A. Tolvanen, K. Nordlund, J. Keinonen, *Phys. Rev. B* **2010**, *81*, 153401.
- [52] K. A. Stephani, I. D. Boyd, *Nucl. Instrum. Methods Phys. Res. B* **2015**, *365*, 235.
- [53] S. Ghaderzadeh, S. Kretschmer, M. Ghorbani-Asl, G. Hlawacek, A. V. Krasheninnikov, *Nanomaterials* **2021**, *11*, 1214.
- [54] S. Gupta, P. Periasamy, B. Narayanan, *Nanoscale* **2021**, *13*, 8575.
- [55] A. V. Krasheninnikov, *Nanoscale Horizons* **2020**, *5*, 1447.
- [56] K. Yoon, A. Rahnamoun, J. L. Swett, V. Iberi, D. A. Cullen, I. V. Vlasiouk, A. Belianinov, S. Jesse, X. Sang, O. S. Ovchinnikova, A. J. Rondinone, R. R. Unocic, A. C. T. van Duin, *ACS Nano* **2016**, *10*, 8376.
- [57] A. A. El-Barbary, R. H. Telling, C. P. Ewels, M. I. Heggie, P. R. Briddon, *Phys. Rev. B* **2003**, *68*, 144107.
- [58] A. V. Krasheninnikov, P. O. Lehtinen, A. S. Foster, R. M. Nieminen, *Chem. Phys. Lett.* **2006**, *418*, 132.
- [59] G.-D. Lee, C. Z. Wang, E. Yoon, N.-M. Hwang, D.-Y. Kim, K. M. Ho, *Phys. Rev. Lett.* **2005**, *95*, 205501.
- [60] F. Banhart, J. Kotakoski, A. V. Krasheninnikov, *ACS Nano* **2011**, *5*, 26.
- [61] C. P. Ewels, R. H. Telling, A. A. El-Barbary, M. I. Heggie, P. R. Briddon, *Phys. Rev. Lett.* **2003**, *91*, 025505.
- [62] A. Gulans, A. Krasheninnikov, M. Puska, R. Nieminen, *Phys. Rev. B* **2011**, *84*, 024114.
- [63] L. Li, S. Reich, J. Robertson, *Phys. Rev. B* **2005**, *72*, 184109.
- [64] F. Banhart, *Rep. Prog. Phys.* **1999**, *62*, 1181.